Modeling of non-structural carbohydrate dynamics by the spatially explicitly individual-based dynamic global vegetation model SEIB-DGVM (SEIB-DGVM-NSC ver1.0)

Hideki Ninomiya[1], Tomomichi Kato[2], Lea Végh[2], and Lan Wu[3]

[1]Graduate School of Global Food Resources, Hokkaido University, Sapporo, Hokkaido 060-0809, Hokkaido, Japan

[2]Research Faculty of Agriculture, Hokkaido University, Sapporo, Hokkaido 060-8589, Japan

[3]College of Ecology and Environment, Hainan University, Hainan, China

Correspondence: Tomomichi Kato (tkato@cen.agr.hokudai.ac.jp)

Tel & Fax: +81 11 706 4942

Abstract. Forest dynamics need to be considered when estimating the global carbon budget. The alteration of forest structure and function under a changing climate and expanding human activity could lead to a reduction of forest canopy cover and a spread of lower-biomass ecosystems in warm and dry regions. Non-structural carbohydrate (NSC) acts as a storage buffer between carbon supplied by assimilation and carbon consumed by, inter alia, respiration, reproduction, and pests. Estimation of NSC concentrations in a tree is very important for accurate projection of future forest dynamics. We developed a new NSC module for incorporation into a spatially explicit, individual-based, dynamic global vegetation model (SEIB-DGVM) to validate the simulated NSC dynamics with observations. NSC pools were simulated in three plant organs: leaves, trunk, and roots. The seasonal dynamics of the NSCs varied among plant species, and the sizes of the NSC pools inferred from observations differed between the boreal, temperate, and tropical climates. The NSC models were therefore validated for each of the three climatic regions at both point and global scales to assess the performance of the models. The modeled NSCs showed good agreement in seasonality with the observed NSCs at four sites—Canada (boreal), Austria and Switzerland (temperate), and Panama (tropical)—and in mean values for three climate zones derived from the global NSC dataset. The SEIB-DGVM-NSCv1.0 is expected to enable simulation of biome shifts caused by the changes of NSC dynamics worldwide. These dynamics will contribute to changes of not only the global carbon cycle but also of forest structure and demography at a global scale.

1 Introduction

Permanent shifts in forest vegetation dynamics have already been observed and are expected to accelerate under future changes of climate globally (McDowell et al., 2020). Forest dynamics are changing due to anthropogenic drivers, such as rising temperatures and CO_2 partial pressures, and are affected by transient disturbances such as wildfires, droughts, biotic attacks, and land-use changes. The dependence of tree recruitment and growth on anthropogenic drivers and transient disturbances could lead to an increase of tree mortality rates in warm and dry regions (Stevens-Rumann et al., 2018; Xu et al., 2017). These changes will cause forests to become shorter and younger. The result will be a net reduction of forest canopy cover and a shift toward low-biomass ecosystems. Furthermore, higher tree mortality will have a negative impact on global ecosystem: lower biological diversity and altered hydrological and carbon cycles (Adams et al., 2013). Understanding the drivers of vegetation dynamics requires accurately simulating the effect of climate change on global terrestrial biogeochemistry.

To increase their chance of survival, trees control their carbon resources and strategically allocate them to growth, respiration, storage, reproduction, and defense (Hoch et al., 2003; Hartmann et al., 2018). When the atmospheric partial pressure of CO_2 increases, trees can allocate surplus carbon to either growth or carbon storage (Hoch et al., 2003; Huang et al., 2020). Changes in tree carbon allocation patterns have been shown to exert large effects on constituents of the terrestrial carbon cycle (Klein and Hoch, 2015). Clarification of the importance of carbon allocation has revealed that non-structural carbohydrates (NSCs) draw much from the other carbon resources because they are the most significant carbon compounds involved in the life processes of trees (He et al., 2020).

The NSC is comprised of starch and sugars, which are mobilized mainly for growth and metabolism when sink strength exceeds source activity (Gough et al., 2010; Richardson et al., 2013; Chuste et al., 2020; Herrera-Ramírez et al., 2020). During photosynthesis, freshly assimilated carbon is transported as triose phosphate from the chloroplast to the cytosol, where sucrose is synthesized from it. Some of the sucrose is then changed into starch in the chloroplast, and the starch is consumed to maintain growth and metabolism at times when recently assimilated carbon is not available to the plants (Dietze et al., 2014). Plants that seasonally shed leaves need to rely on stored carbon for maintenance during the leafless season. NSCs play an important role as substrates for the synthesis of compounds in plants and as energy sources for metabolic activities (Hartmann et al., 2018). Moreover, NSCs include key compounds that are used to buffer physiological stress when energy from photosynthesis does not satisfy metabolic demands (Gough et al., 2010; Sala et al., 2012) because carbohydrates such as starch can be easily mobilized and reallocated (Hartmann et al., 2018).

72   In long-lived plants, the ability to store carbon is a key to survival at times when
73   photosynthetic rates are low because of shade, drought, and disturbance (Martínez-Vilalta et al.,
74   2016). As a result, the amount of NSC storage or remobilization depends on the balance between
75   the supply and demand of assimilated carbon and accounts for a large fraction of the annual carbon
76   budget of plants (Richardson et al., 2013). When carbon allocation patterns favor storage over
77   growth, tree growth is limited (Wang et al., 2021). Hence, the dynamics of stored carbon pools
78   can be considered an indicator of the carbon balance of the plant.

79   The decline of stomatal conductance during a drought reduces photosynthetic carbon
80   assimilation and thus decreases the amount of NSC (McDowell et al., 2008; Adams et al., 2017).
81   Although an imbalance of the NSC pool could mechanistically trigger plant mortality, few
82   ecological models predict tree mortality resulting from the role of NSC associated with climate
83   change (Adams et al., 2013; McDowell, 2011). Simulations of the NSC dynamics of plants will
84   elucidate the effects of different drivers on forested ecosystems (Gough et al., 2010).

85   Because the frequency, duration, and severity of droughts are expected to increase globally,
86   the damage to plants through rising temperatures, water vapor pressure deficit, and associated
87   water loss will also increase (IPCC, 2014; Sevanto and Dickman, 2015). Trees can be killed
88   directly by drought, i.e. vial desiccation, or indirectly by associated increases of insect or pathogen
89   attacks. Indirect effects that cause tree mortality include girdling by bark beetles and defoliation
90   events. The frequency and severity of this indirect biotic disturbance from insects and insect–
91   pathogen complexes have been increasing (McDowell et al., 2020; Seidl et al., 2017). According
92   to multiple observational and experimental studies, the resulting imbalance between NSC demand
93   and supply leads to carbon starvation, which is one of the mechanisms that contribute to drought-
94   induced mortality (McDowell, 2011).

95   Dynamic global vegetation models (DGVMs) are often used to represent vegetation dynamics
96   as well as biogeochemical cycles and to simulate the transition of the vegetation structure in
97   response to climatic changes via modeling of competition and disturbance (Hickler et al., 2004;
98   Krinner et al., 2005; Braakhekke et al., 2019). In DGVMs, plant species are classified into plant
99   functional types (PFTs) based on their eco-physiological traits. However, most DGVMs
100 oversimplify individual plant competition by using average values of traits for each PFT (Smith
101 et al., 2001). Most of such models miss the effects of local competition for light, which must be
102 considered when modeling gap population dynamics among individual trees (Sato et al., 2007).

103 In contrast, the Spatially Explicit, Individual-Based, Dynamic Global Vegetation Model
104 (SEIB-DGVM; Sato et al., 2007) can simulate the growth of individual trees on numerous
105 replicate patches and enable observation of how single, large trees can influence nearby trees.
106 Plants in different patches do not interact with each other in terms of physical resources such as
107 light and water. In each patch, the growth and mortality of each tree, and competitive interactions

108 between individual trees are calculated based on environmental conditions. Transient changes in
109 vegetation distribution and dynamics can therefore be examined (Sato et al., 2007). Because the
110 amount of stored NSC depends on the size of individual trees and because the SEIB-DGVM can
111 simulate individual trees, we chose the SEIB-DGVM to estimate the NSC dynamics of plants.

112   SEIB-DGVM has been used to simulate a transient change in the distribution and function of
113 vegetation on the African continent in conjunction with the ranges of dispersal of trees and to
114 address factors that had a strong impact on the transient change (Sato and Ise, 2012). Use of the
115 SEIB-DGVM has enabled reconstruction of the geographical distributions of plant productivity
116 and thermo-hydrology based on observations in eastern Siberia and partial representation of the
117 effect of topography on the abundance of trees in larch forests (Sato et al., 2020). The SEIB-
118 DGVM was coupled with an earth system model (MIROC-ESM; Watanabe et al., 2011).

119   However, the original SEIB-DGVM lacks the ability to compute NSC levels in trees, which
120 means it cannot simulate the plant death caused by an imbalance in the NSC pool, as well as
121 indirect impacts like insect infestations and defoliation. This also hinders the ability to investigate
122 the effects of various drivers on forest ecosystems, such as the intensification of drought, and
123 limits the development of the MIROC-ESM for simulating the global carbon cycle.

124   The objectives of the research were to 1) incorporate a module to simulate NSC dynamics in
125 the SEIB-DGVM and 2) validate the simulated NSC dynamics with observational data at both
126 point and global scales. We therefore created a new function in the SEIB-DGVM to represent the
127 NSC dynamics of individual trees. How NSC is produced, stored, and distributed among different
128 plant organs under environmental stress is poorly understood (Jones et al., 2019; Rademacher et
129 al., 2021; Wang et al., 2021). Our enhanced model improves the physiological simulation of the
130 leaf life cycle and enhances understanding of how NSC affects the distribution of vegetation,
131 gross primary production (GPP), and net primary production (NPP) as well as tree dynamics (age,
132 height, and trunk diameter) at global scales in the future. By adjusting the NSC accumulation
133 rates of individual trees and the threshold of NSC-induced mortality during drought, the model
134 can simulate the timing, location, and percentage of trees that die in response to moderate drought.
135 Furthermore, the model can increase our understanding of the role of NSCs.

136

137 **2 Model**

138

139 **2.1 Spatially Explicit Individual-Based Dynamic Global Vegetation Model (SEIB-DGVM)**

140

141 The SEIB-DGVM (v3.02; http://seib-dgvm.com/data/seib_code302.zip; Sato et al., 2016) is a
142 carbon budget model that simulates the establishment of individual trees, competition between
143 trees, and the death of individual trees according to input climate data. The default settings follow

144   the structure of a three-dimensional virtual forest on a 30 m × 30 m stand of trees with 1 m × 1 m

145   simulation grid cells. In each grid cell, a tree belonging to one of 14 woody plant functional types

146   (PFTs) is assigned depending on conditions, in addition to one of 2 grass PFTs. All physical and

147   physiological processes are calculated at daily time steps, trunk growth is estimated monthly, and

148   vegetation dynamics and disturbance such as wildfire and heat stress are assessed annually.

149   Because of the lack of field observations at the time the model was developed, there is no

150   mechanism to control the NSC in leaves and roots in the original SEIB-DGVM, and only the NSC

151   in trunks is simulated after adjusting the available organic matter for reproduction and respiration.

152   The original SEIB-DGVM therefore cannot represent NSC-induced effects on forest ecosystems

153   realistically without accounting for the NSC in leaves and roots.

154

155   **2.2 NSC components**

156

157   **2.2.1 NSC pool**

158   The new NSC pools are separated into three organs of an individual tree: leaves, trunk, and roots.

159   In the original SEIB-DGVM, the NSC in trunks is supplemented to 250 g dry matter (DM) from

160   the litter after seed establishment and is based on the existing leaf biomass after the first 30 days

161   of the growing season. It is used for foliation after the dormant phase and metabolic processes

162   such as the synthesis of a storage organ and remobilization of the nutrients within it. In the new

163   model, the carbon newly assimilated via photosynthesis goes into three NSC pools. The NSC

164   pools can be later mobilized for growth and respiration as follows (Fig. 1).

165

166     $\Delta NSC_t = NPP_t = \Delta NSC_{trunk,t} + \Delta NSC_{leaf,t} + \Delta NSC_{root,t},$ (1)

167

168   when $NSC_{trunk,\,t-1} < NSC_{trunk,\,max(t)}$, $NSC_{leaf,\,t-1} < NSC_{leaf,\,max(t)}$, and $NSC_{root,\,t-1} < NSC_{root,\,max(t)}$,

169

170
$$\begin{cases} \text{parent } NSC_{trunk,t} = \min\left(NSC_{trunk,max\,(t)}, \Delta NSC_t\right), \\ \quad\quad NSC_{leaf,t} = \min\left(NSC_{leaf,max\,(t)}, \Delta NSC_t - NSC_{trunk,t}\right), \\ \quad\quad NSC_{root,t} = \min\left(NSC_{root,max(t)}, \Delta NSC_t - NSC_{trunk,t} - NSC_{leaf,t}\right), \end{cases}$$
    (2)

171

172   when $NSC_{trunk,\,t-1} < NSC_{trunk,\,max(t)}$, $NSC_{leaf,\,t-1} < NSC_{leaf,\,max(t)}$, and $NSC_{root,\,t-1} > NSC_{root,\,max(t)}$

173

174
$$\begin{cases} NSC_{trunk,t} = \min\left(NSC_{trunk,max(t)}, \Delta NSC_t\right), \\ NSC_{leaf,t} = \min\left(NSC_{leaf,max(t)}, \Delta NSC_t - NSC_{trunk,t}\right), \\ NSC_{root,t} = NSC_{root,max(t)} \\ \quad\quad\quad\quad\quad\quad , \end{cases}$$
    (3)

175

when $NSC_{trunk, t-1} < NSC_{trunk, max(t)}$, $NSC_{leaf, t-1} > NSC_{leaf, max(t)}$, and $NSC_{root, t-1} < NSC_{root, max(t)}$,

177

$$\begin{cases} NSC_{trunk,t} = \min(NSC_{trunk,max(t)}, \Delta NSC_t), \\ NSC_{leaf,t} = NSC_{leaf,max\,(t)}, \\ NSC_{root,t} = \min(NSC_{root,max(t)}, \Delta NSC_t - NSC_{trunk,t} - NSC_{leaf,t}), \end{cases} \tag{4}$$

179

when $NSC_{trunk, t-1} < NSC_{trunk, max(t)}$, $NSC_{leaf, t-1} > NSC_{leaf, max(t)}$, and $NSC_{root, t-1} > NSC_{root, max(t)}$,

181

$$\begin{cases} parent\ NSC_{trunk,t} = \min(NSC_{trunk,max(t)}, \Delta NSC_t), \\ NSC_{leaf,t} = NSC_{leaf,max\,(t)}, \\ NSC_{root,t} = NSC_{root,max\,(t)}, \end{cases} \tag{5}$$

183

when $NSC_{trunk, t-1} > NSC_{t, max(t)}$, $NSC_{leaf, t-1} < NSC_{leaf, max(t)}$, and $NSC_{root, t-1} < NSC_{root, max(t)}$,

185

$$\begin{cases} NSC_{trunk,t} = NSC_{t,max(t)} \\ NSC_{leaf,t} = \min(NSC_{leaf,max\,(t)}, \Delta NSC_t), \\ NSC_{root,t} = \min(NSC_{root,max(t)}, \Delta NSC_t - NSC_{trunk,t} - NSC_{leaf,t}), \end{cases} \tag{6}$$

187

when $NSC_{trunk, t-1} > NSC_{t, max(t)}$, $NSC_{leaf, t-1} < NSC_{leaf, max(t)}$, and $NSC_{root, t-1} > NSC_{root, max(t)}$,

189

$$\begin{cases} NSC_{trunk,t} = NSC_{t,max(t)}, \\ NSC_{leaf,t} = \min(NSC_{leaf,max\,(t)}, \Delta NSC_t), \\ NSC_{root,t} = NSC_{root,max(t)}, \end{cases} \tag{7}$$

191

when $NSC_{trunk, t-1} > NSC_{t, max(t)}$, $NSC_{leaf, t-1} > NSC_{leaf, max(t)}$, and $NSC_{root, t-1} < NSC_{root, max(t)}$,

193

$$\begin{cases} NSC_{trunk,t} = NSC_{t,max(t)}, \\ NSC_{leaf,t} = NSC_{leaf,max(t)}, \\ NSC_{root,t} = \min(NSC_{root,max\,(t)}, \Delta NSC_t), \end{cases} \tag{8}$$

195

when $NSC_{trunk, t-1} > NSC_{t, max(t)}$, $NSC_{leaf, t-1} > NSC_{leaf, max(t)}$, and $NSC_{root, t-1} > NSC_{root, max(t)}$,

197

$$\begin{cases} NSC_{trunk,t} = NSC_{t,max(t)}, \\ NSC_{leaf,t} = NSC_{leaf,max(t)}, \\ NSC_{root,t} = NSC_{root,max\,(t)}, \end{cases} \tag{9}$$

199

200   where t is the calculation day, t-1 is the previous day, NSC_{organ} is the amount of NSC in each organ,

201   and $NSC_{organ, max(t)}$ is the maximum amount of NSC in each organ on day t.

202   The NSC pools of the organs displays unique seasonality for each climatic zone. The NSC

203   seasonality of each organ varies among tree species mainly because the climate and surrounding

204   environment influence the capacity and utilization of NSCs in plants. To take into consideration

205   the fact that field observations of NSC covered whole seasons and that various plant species were

206   scarce, we classify NSC seasonality into three types: tropical, temperate, and boreal. Observations

207   from temperate forests showed that the NSC seasonal cycles were similar among the organs and

208   peaked around late spring–summer, although the NSC_{organ} differed in size (Hoch et al., 2003;

209   Richardson et al., 2013; Woodruff and Meinzer, 2011; Gruber et al., 2012). In contrast, the NSC

210   concentrations in the leaves of boreal trees peak in June (Sveinbjörnsson et al., 2010), and NSCs

211   in the fine roots increase until summer and then decline toward mid-summer and fall because of

212   the initiation of root growth (Landhäusser and Lieffers, 2003). All 14 woody PFTs of the SEIB-

213   DGVM are sorted into one of three NSC types, and carbon assimilated via photosynthesis was

214   allocated to the NSC pool of each organ in temperate and boreal PFTs as follows.

215

216    $$NSC_{organ, max} = (a + b \times \text{daily GPP}) \times \text{Biomass},\qquad(10)$$

217

218   where the organ is either a leaf, trunk, or root, a is the minimum value, and b is the seasonality

219   parameter.

220   Tropical species have a different NSC seasonality from temperate and boreal species. The

221   NSC of leaves display a concave upward seasonal pattern that reaches its minimum in late spring–

222   early summer (Würth et al., 2005), which is a dry season when leaf production and flowering

223   deplete NSC pools. Singh and Srivastava (1986) have observed that the NSC of roots is at a

224   minimum level from July to September because the NSC pool is drained to enable survival of the

225   rainy season during that period. The amount of NSCs then increases toward winter, when the fine

226   root biomass declines. Hence, Eq. (10), which is used for temperate and boreal forests, is

227   inadequate for simulation of tropical forests because the NSC depends less on the seasonality of

228   photosynthesis in the tropics. The size of the NSC pool of tropical species therefore accumulates

229   as follows.

230

231    $$NSC_{organ, max} = (a + b) \times \text{Biomass},\qquad(11)$$

232

233   where the organ is either the leaf, trunk, or root, a is the minimum value, and b is the seasonality

234   parameter.

235  First, the surplus carbon that remains after respiration is assigned to the NSC_{trunk} using Eq.

236 (1). Once NSC_{trunk} has reached its maximum capacity, the rest of assimilated carbon moves

237 primarily into NSC_{leaf}, secondarily into NSC_{root}. Finally, any remaining carbon is allocated to the

238 growth of leaves, the trunk, and roots. The sum of the NSCs in the leaves, trunk, and roots (the

239 total NSC) is maximized in relation to total biomass for each climate region (Table 1). In cases

240 where the total NSC exceeds this upper limit, the surplus is directly consumed for the growth of

241 each organ.

242

243 

Table 1. Maximum volume of NSC pool

Maximum of NSC pool		
Boreal	10% of total biomass	Martínez-Vilalta et al. (2016)
Temperate	5% of total biomass	Hoch et al. (2003)
Tropical	9% of total biomass	Würth et al. (2005)

244

245 **2.2.2 NSC expenditure**

246

247 **2.2.2.1 Respiration**

248

249 Normally, photosynthetically assimilated carbon is used for maintenance respiration without

250 entering the NSC pool. When the assimilated carbon is insufficient for maintenance respiration,

251 the NSC compensates for the shortage. The NSC loss is allocated to each organ as follows.

252

253 $NSC_{leaf, t} = NSC_{leaf, t-1} - R_{a, t-1} \times c_{leaf}$      (12)

254 $NSC_{trunk, t} = NSC_{trunk, t-1} - R_{a, t-1} \times c_{trunk}$     (13)

255 $NSC_{root, t} = NSC_{root, t-1} - R_{a, t-1} \times c_{root},$      (14)

256

257 where autotrophic respiration (R_a) is the difference between assimilated carbon and maintenance

258 respiration and c is the allocation factor for NSC utilization ($c_{leaf} + c_{trunk} + c_{root} = 1$). If the total

259 NSC equals the carbon shortfall, the NSC of all organs becomes zero. If an NSC_{organ} is insufficient

260 to provide the allocated share of R_a, the other organs will supply the difference: the NSC_{leaf} is

261 supplemented first from the NSC_{trunk}, and if that is not enough, from the NSC_{root}. Similarly, if any

262 of the other NSC_{organ} pools is unable to cover local shortages, the NSC pools of the remaining

263 organs will balance the supply and demand. When the total NSC is not enough to pay for the

264 charges, a 1% of reduction in the biomass of all of the living organs occurs. The removed biomass

265 of sapwood is transformed into heartwood, while the removed biomass of other organs is placed

266 into the litter pool. The allocation factors of NSC utilization depend on the climatic region (Table

267 2), and have been adjusted to prevent the allocated share of R_a from hindering an increase in
268 NSC_{organ} during spin-up simulations.
269
270

Table 2. Allocation ratio (c) of NSC to organs

Organ	Boreal	Temperate	Tropical
Leaf	0.20	0.05	0.01
Trunk	0.60	0.90	0.98
Root	0.20	0.05	0.01

271
272 **2.2.2.2 Phenology**
273
274 In SEIB-DGVM, every deciduous PFT has two phenology phases: a growth phase and a dormant
275 phase. The NSCs are consumed for foliation after the dormant phase. The NSC is allocated at the
276 rates shown in Table 2.
277
278 **2.2.2.3 Turnover**
279
280 Part of the NSC pools of leaves and roots is transformed into litter at the same fractional rates as
281 in the turnover of general carbon pools for leaves and roots. This turnover is calculated at daily
282 steps, regardless of the phenology phase.
283
284 **2.2.2.4 Establishment**
285
286 The establishment process is performed on the last day of each simulation year in the SEIB-
287 DGVM. The characteristics of the PFT are determined by five bioclimatic parameters: (1) the
288 maximum temperature in the coldest month; (2) the maximum growing-degree day; (3) the
289 minimum growing-degree day; (4) the minimum photosynthetically active radiation; and (5) the
290 duration of drought. All new trees, independent of their PFT, start with a sapwood diameter of
291 0.01 m and heartwood diameter of 0.00 m. Initially, these new trees have no leaves or fine roots.
292 Their carbon cycle is therefore maintained by initial values of 250 g DM of assimilated carbon
293 and 250 g DM of NSC (NSC_{leaf} = 10 g, NSC_{trunk} = 190 g, and NSC_{root} = 50 g) from the litter pool.
294
295 **2.3 Validation of NSC for point and global simulations**
296
297 Observational NSC data for model validation were derived from Martínez-Vilalta et al. (2016),
298 who reviewed 296 papers and summarized NSC dynamics in forests. Their data include total

299 NSCs in leaves, trunks, and roots of mature terrestrial plants from observations over at least four
300 months. The new model was first validated at the point scale. After confirming that the model can
301 accurately simulate at the point scale, it was then validated at the global scale. These data were
302 used for both point-scale and global-scale model validations. For the point-scale simulation,
303 several field sites were selected, which NSC data were available for all organ. At each site, the
304 seasonality of the NSC was measured for at least four months. The modeled outputs were then
305 compared to the observed data, which were calculated using local climate data on a grid that
306 corresponds to the field site. For the global-scale simulation, global mean NSC values derived by
307 using all observed data from the relevant climate zones. The modeled outputs calculated using
308 $0.5° \times 0.5°$ gridded climate data were then compared to these values.
309
310 **2.3.1 Validation at a point scale**
311
312 **2.3.1.1 Site descriptions**
313
314 Four countries were used to validate the simulated NSC content in the plant organs: boreal
315 (Canada), temperate (Austria and Switzerland), and tropical (Panama). We used local climate data
316 from meteorological stations gap-filled by corrected gridded climate reanalysis data as the input
317 at these sites. We ran the NSC module including the SEIB-DGVM with the location and climate
318 provided and compared the model output with the observation data.
319   The boreal site is located near Alder Flats, Alberta, Canada (52°58'N, 114°59'W) in 2000. The
320 site was dominated by boreal winter deciduous plants such as *Populus tremuloides* (Landhäusser
321 and Lieffers, 2003). One of the temperate sites is located in the timberline ecotone at Mt.
322 Patscherkofel to the south of Innsbruck, Austria (47°13′N, 11°27′E) in 2008 (Gruber et al., 2011).
323 Temperate conifer species such as *Pinus cembra* were the dominating tree species. The other
324 temperate site is at the Mont Noble, Canton Valais, Swiss Central Alps (46°12′N, 7°30′E) and was
325 dominated by temperate conifers (*P. cembra* L.; Hoch et al., 2003) in 2000. The tropical site is
326 located at the Parque Natural Metropolitano near Panama City, the Republic of Panama in 1996
327 (85°8′N, 79°34′W; Würth et al., 2005). The site has mixed cover with 17 dominant species,
328 including *Cecropia longipes* and *Anacardium excelsum*.
329
330 **2.3.1.2 Input climate data**
331
332 The SEIB-DGVM requires ten climatic variables as environmental drivers: air temperature, soil
333 temperature at a depth of 50 cm (soil layer 1), soil temperature at a depth of 100 cm (soil layer
334 2), soil temperature at a depth of 150 cm (soil layer 3), precipitation, shortwave radiation,

335 longwave radiation, wind velocity, specific humidity, and diurnal range of air temperature. The

336 input climate data were prepared by harmonizing a global reanalysis gridded climate dataset, the

337 WATCH Forcing Data ERA-Interim (WFDEI, 0.5 × 0.5 degrees, 1979–2016,

338 Weedon et al., 2018), and the climate generated by the SEIB generator (Tei et al., 2017), which

339 is the monthly observation-based climatic datasets produced by Climatic Research Unit (CRU

340 TS4.00, 0.5 × 0.5 degrees, 1901-2015, Harris et al., 2014) supplemented with the National

341 Centers for Environmental Prediction/National Center for Atmospheric Research

342 (NCEP/NCAR) daily climate datasets (Kalnay et al., 1996) for 1950, with local climatology

343 recorded at meteorological stations near the sites. Local climatology in Panama is measured at

344 the Parque Natural Metropolitano Canopy Crane meteorological station (1995–2019). The

345 climatology in Austria (1979–2008) and Switzerland (1979–2000) was derived from the closest

346 meteorological station to the field site under the European Climate Assessment (Klein et al.,

347 2002, https://www.ecad.eu). WFDEI data were used for the climatology in Canada, except for

348 precipitation data, which are measured in the Meteorological Service of Canada (1979–1984,

349 https://climate.weather.gc.ca/historical_data/search_historic_data_e.html).

350   The reanalysis of daily WFDEI and SEIB climate data included daily records, which were

351 corrected by regression models to local climate data. For temperature, humidity, and shortwave

352 radiation values, local climatology were used directly and the daily WFDEI data supplemented

353 by simple linear regression. Precipitation data and wind speeds were first adjusted to monthly and

354 then annual averages and then scaled as a correction. WFDEI precipitation data were scaled after

355 adjusting to the annual climatological precipitation of 995 mm in 2008 for Austria and 630 mm

356 in 2000 for Switzerland. Longwave radiation was calculated using harmonized temperatures and

357 humidities above (Brutsaert, 1975). Missing values were estimated via linear interpolation.

358 Because soil temperature data were unavailable for local sites and for WFDEI, soil layer

359 temperatures were calculated using the SEIB generator by regressing soil layer 1 on atmospheric

360 temperature, soil layer 2 on layer 1, and layer 3 on layer 2. In Austria, humidity data were available

361 from 2005. The WFDEI data were therefore used to estimate missing data via linear interpolation.

362 In Canada, no observational data were available, except for temperature and precipitation.

363 Precipitation in Canada was scaled with WFDEI data after adjusting to the total climatological

364 precipitation for 1979–1984, shortwave radiation was taken from the WFDEI, and humidity data

365 were harmonized in the same way as the humidity data in Austria.

366

367 **2.3.1.3 Simulation scheme**

368

369 To reach equilibrium conditions of the biomes, plant, and soil carbon pools, a 1000-year spin-up

370 simulation was performed by looping the climate data and atmospheric CO_2 concentrations

371   between 1979–2000. Building on the final conditions of the spin-up simulations, continuous

372   simulations corresponding to 1979–2001 in Canada, 1979–2008 in Austria, 1979–2000 in

373   Switzerland, and 1979–1995 in Panama were carried out, and the NSC dynamics were compared

374   with field data.

375

376   **2.3.2 Validation at a global scale**

377

378   In the global-scale simulation, the NSC seasonality in the SEIB-DGVM was validated using

379   CRU/NCEP/MIROC integrated data (0.5 × 0.5 degrees, 1850-2100, Tei et al., 2017, Watanabe et

380   al., 2011) as climatic input. SEIB-DGVM-NSC ver 1.0 is expected to simulate on future scenarios,

381   thus the different climate data that cover longer period than that of section 2.3.1.2. are used for

382   validation at a global scale. The SEIB-DGVM categorizes plant species into 16 PFTs for global-

383   scale simulations.

384   The outputs of the SEIB-DGVM include two boreal biome types (evergreen and deciduous

385   forests), three temperate biome types (conifer, broad-leaved evergreen, and deciduous forests),

386   and two tropical biome types (evergreen and deciduous forests), whereas the observations

387   included two boreal biome types (conifer and deciduous forests), three temperate biome types

388   (conifer, evergreen, and deciduous forests), and two tropical biome types (evergreen and

389   deciduous forests). The model outputs and observation data were compared for each climate zone.

390   Global climate data were available from 1850 to 2005. The first 30 years (1850–1880) were

391   therefore looped for a 1000-year spin-up simulation. After the spin-up, simulations were run for

392   the period 1850–2005. The NSC dynamics from the period 1975–2005 were used for model

393   validation.

394

395   **2.4 Parameterization of NSC functions**

396

397   Hoch et al. (2003) have reported that the NSC_{leaf} of temperate trees sampled near the village of

398   Hofstetten in Switzerland varies between 7%–20% of the total leaf DM. They determined the

399   seasonal mean of the NSC_{trunk} in sapwood of temperate deciduous trees and temperate evergreen

400   trees to be 4.7% ± 0.1% of DM and 1.8% ± 0.1% of DM, respectively. There were no significant

401   seasonal differences. The mean NSC_{root} was less than 1.5% of the root DM for forests in Austria

402   throughout the whole season (Gruber et al., 2012), and the total NSC of temperate trees was

403   around 4%–5% of the DM during the growing season (Gruber et al., 2011). For tropical trees

404   collected in Parque Natural Metropolitano in Panama, the NSC_{trunk} and NSC_{root} were 8%–10% of

405   their biomass, whereas the NSC_{leaf} fluctuated within 5%–9% of leaf biomass (Würth et al., 2005).

406   Landhäusser and Lieffers (2003) have reported that the NSC_{root} of boreal trees in Canada, which

407 is used to support leaf flush and root growth, is 3%–4% of their root mass. The stemwood NSC_{trunk}

408 concentration is ~18 mg g^{-1} of the DM for sample forests collected by Ameri flux tower (Carbone

409 et al., 2013). Because of limited observational data, the parameters of the NSC processes were

410 derived mostly from the values observed at each site used for point-scale validation, and the

411 maximums of simulated NSCs were corrected so that they were in the range of measured NSCs.

412   First, the parameter a in Eq. (10) controls the base amount of photosynthetically fixed carbon

413 mobilized for the NSC pools. The parameter b in Eq. (10) controls the seasonal fluctuations of

414 the NSCs from the parameter a. In temperate zones, the value of b differs before and after July so

415 that NSC peaks around mid-summer. In contrast, in tropical zones, the amount of NSC in leaves

416 and trunks decreases throughout the spring–summer.

417   The same parameter a and b were basically used for global-scale validation as for point-scale

418 validation. However, because the NSCs are influenced by environmental conditions at the field

419 sites, the observed global mean values used for global-scale validation were different from the

420 values used for setting parameters for point-scale validation. Therefore, some adjustments were

421 made to certain parameters to align with the values used in the global-scale validation. Tables 3

422 and 4 show the parameters used for validation. Parameter values unrelated to the NSC module

423 remain at the default values of the SEIB-DGVM (Sato et al., 2007).

424

425   **Table 3.** Parameters of NSC pool size function for point-scale simulation

Organ	Canada	Austria	Switzerland	Panama
Leaf	a: 0.09, b: 0.4 $\times 10^{-3}$	a: 0.04, b: 0.065 $\times$ 10^{-3} (Jul–Oct) a: 0.04, b: 0.135 $\times$ 10^{-3} (others)	a: 0.13, b: 0.1 $\times 10^{-3}$ (Jul–Oct) a: 0.13, b: 0.7 $\times 10^{-3}$ (others)	a: 0.06, b: $-0.15 \times$ 10^{-3} (Jun–Nov) a: 0.06, b: 0.15 $\times 10^{-3}$ (others)
Trunk	a: 0.06, b: 0.03 $\times 10^{-3}$	a: 0.02, b: 0.05 $\times 10^{-3}$	a: 0.02, b: 0.01 $\times$ 10^{-3}	a: 0.1, b: -0.25×10^{-3} (Jun–Nov) a: 0.1, b: 0 (others)
Root	a: 0.14, b: 0.06 $\times 10^{-3}$	a: 0.02, b: 0.01 $\times 10^{-3}$	a: 0.06, b: 0.003 $\times$ 10^{-3}	a: 0.04, b: 0.5 $\times 10^{-3}$

426

427

428   **Table 4.** Parameters of NSC pool size functions for global-scale simulation

Organ	Boreal	Temperate	Tropical
Leaf	a: 0.09, b: 0.4 $\times 10^{-3}$	a: 0.13, b: 0.1 $\times 10^{-3}$ (Jul–Oct) a: 0.13, b: 0.9 $\times 10^{-3}$ (others)	a: 0.06, b: -0.15×10^{-3} (May–Jul) a: 0.06, b: 0.15 $\times 10^{-3}$ (others)

Trunk	a: 0.06, b: 0.03 × 10⁻³	a: 0.04, b: 0.01 × 10⁻³	a: 0.1, b: −0.13 × 10⁻³(May–Jul)
			a: 0.1, b: 0 (others)
Root	a: 0.14, b: 0.06 × 10⁻³	a: 0.06, b: 0.003 × 10⁻³	a: 0.04, b: 0.5 × 10⁻³

429

430
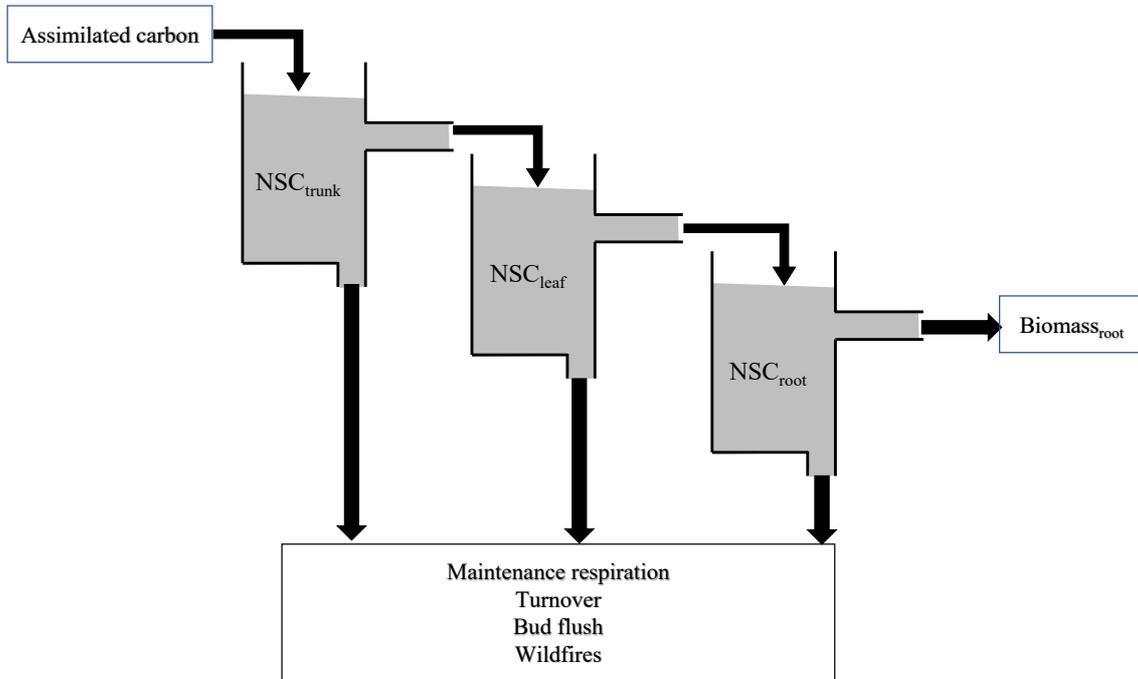
Figure 1. Schematic model structure of NSC pool. The assimilated carbon satisfies the NSC_{trunk}, and then the excess assimilated carbon satisfies the next NSC_{leaf} and NSC_{root}. The accumulated carbon in NSC pool is used to compensate for the shortage of maintenance respiration and help with bud flush, and is sometimes lost due to turnover. When the biomass of plants is lost due to wildfires, the NSC also decreases.

431
432
433
434
435
436
437
438
439

3 Results

3.1 Seasonality of NSC at the point scale

3.1.1 Boreal

In Canada, the fact that the dominant PFT in the simulations was boreal deciduous trees was consistent with observations at the site in Canada. The model simulated an increase in the NSC of leaves from 80 mg g^{-1} to 203 mg g^{-1}, whereas the observed NSC values were 89 mg g^{-1} in May and 185 mg g^{-1} in August (Fig. 2a). The modeled NSCs in leaves therefore captured the increasing trend during the growing season, but the simulations overestimated the maximum NSC a little. The observed NSCs in trunks fluctuated from 90 mg g^{-1} to 192 mg g^{-1} during a year with no specific seasonal trend (Fig. 2e). The model outputs in trunks were in the range 56–76 mg g^{-1}. Although the observed fluctuations exceeded the modeled outputs, the modeled outputs were within one standard deviation of the observations. The range of the observed NSCs in roots was 97–138 mg g^{-1}, whereas the range of the modeled NSCs was 117–132 mg g^{-1} (Fig. 2i). However, the observations peaked in August 2001 and in October 2002. The modeled NSCs of roots differed from the observed NSCs because the former peaked during August in both years. Overall, the simulated NSCs agreed well with the observed data (Fig. 3; RMSE = 69.92 mg g^{-1}, r = 0.21).

3.1.2 Temperate

In Austra, the fact that the dominant PFT in the simulations was temperate conifer forests was consistent with observations at the site in Austria. The modeled NSCs in leaves accumulated until July with a maximum of 142 mg g^{-1}. This pattern was similar to the observed seasonality of the NSCs, which peaked at 150 mg g^{-1} (Fig. 2b). The modeled NSCs in trunks were stable in the range 19–26 mg g^{-1}, and the observations were within the range 18–38 mg g^{-1}, with no specific seasonality (Fig. 2f). The modeled values were interspersed between the observations. The modeled NSCs in roots varied in a curvilinear manner from 18 to 26 mg g^{-1}, a range that was similar to the range of the observed NSCs, 13–32 mg g^{-1} (Fig. 2j). The seasonality and magnitudes of the modeled NSCs were consistent with observations (Fig. 3; RMSE = 9.52 mg g^{-1}, r = 0.95).

In Switzerland, the dominant PFT in the simulations corresponded to the temperate conifers observed at the field site. The NSCs in the tree leaves accumulated during early spring and reached up to 222 mg g^{-1} (Fig. 2c). The decrease of the NSCs after July to a minimum of 135 mg g^{-1} was similar to the decline of the observed NSCs to a minimum of 124 mg g^{-1}. The modeled NSCs in trunks fell in the range 13–16 mg g^{-1}, which was overlapped with the range of the observed NSCs in trunks, 15–33 mg g^{-1} (Fig. 2g), and the modeled NSCs all fell within one standard deviation of

476 the observations. The modeled NSCs in roots increased gradually from 45 to 62 mg g^{-1}, which is

477 similar to the observed range of observations, 48–64 mg g^{-1} (Fig. 2k). The simulations captured

478 the amounts and seasonal patterns of the NSCs in the different organs and produced results that

479 compared well with observations (Fig. 3; RMSE = 25.83 mg g^{-1}, $r = 0.91$).

480

481 **3.1.3 Tropical**

482

483 In Panama, while a wide range of woody species was found at the Panama site, in the simulation

484 the tropical evergreen PFT became dominant. The simulations showed that the NSCs in leaves

485 were stored during winter and were then gradually consumed from July to October, when they

486 reached a minimum of 52 mg g^{-1} (Fig. 2d). The observed NSCs in leaves likewise decreased from

487 69 to 48 mg g^{-1} between August and October. The model therefore followed the observed

488 seasonality of the leaf NSCs. The modeled NSCs in trunks fell in the range 35–73 mg g^{-1} (Fig.

489 2h). The slight decrease of the modeled NSCs in trunks during the summer was not apparent in

490 the observations. However, the simulated values fell within the range of the observed NSCs, 27–

491 97 mg g^{-1}. The simulated NSCs in roots fell in the range 23–55 mg g^{-1}; the observed NSCs ranged

492 from 43 to 70 mg g^{-1} (Fig. 2l). Despite the weak correlation between simulated and observed

493 NSCs, the model results were within the acceptable margin of error (Fig. 3; RMSE = 20.75 mg

494 g^{-1}, $r = 0.08$).

495

496 **3.2 Comparison of annual mean NSC concentrations at a global scale**

497

498 For validation at a global scale, the mean annual NSCs from the new model were compared with

499 the observed mean annual NSCs in boreal, temperate, and tropical regions (Table 5). The model

500 simulated the amounts of NSCs in forest tree trunks in all climate regions with high accuracy. The

501 modeled NSCs in the trunks of trees in boreal forests averaged 47.48 ± 18.35 mg g^{-1}, which

502 compared favorably with the observed average of 76.67 ± 23.68 mg g^{-1}. In temperate forests, the

503 modeled NSCs of trunks averaged 44.78 ± 6.82 mg g^{-1}, which was close to the observed average of

504 51.59 ± 22.63 mg g^{-1}. The modeled NSCs of trunks in tropical forests averaged 66.68 ± 18.79 mg g^{-1},

505 which was close to the average of the observations, 106.23 ± 32.52 mg g^{-1}. Although the modeled

506 NSCs in leaves of temperate and tropical forests were close to observed values, the modeled NSCs

507 in leaves of boreal forests underestimated the observed values. Moreover, the modeled NSCs in

508 roots of tropical forests were smaller than the observed NSCs. Overall, the simulated NSCs of all

509 organs of forest trees in all climate regions agreed reasonably well with observations (Fig. 4;

510 RMSE = 66.75 mg g^{-1}, $r = 0.17$). The model could simulate the NSCs with high accuracy, with

511 the exception of the NSCs of tree leaves in boreal forests and of tree roots in tropical forests (Fig.

512   4; RMSE = 34.15 mg g^{-1}, r = 0.71). The original SEIB-DGVM only calculated NSCs in the trunks

513   of trees with, an average value of 63.70 ± 44.64 mg g^{-1} in boreal forests, 20.87 ± 15.91 mg g^{-1} in

514   temperate forests, and 16.61± 10.22 mg g^{-1} tropical forests. Although the NSC in trunks of boreal

515   forests from the original SEIB-DGVM was close to observation, the old model underestimated

516   the NSC in trunks of temperate and tropical forests. The simulated NSCs from the original SEIB-

517   DGVM in all climate regions were found to be poorly less correlated with observations (Fig. 4;

518   RMSE = 55.37 mg g^{-1}, r = 0.01).

519

520   **Table 5.** Comparison of modelled and observed annual mean NSC concentrations (mg g^{-1}) on a

521   global scale. The observed results are represented as the mean ± 1 standard deviation

	Boreal		Temperate		Tropical	
	Observation	Model	Observation	Model	Observation	Model
Leaf	202.80 ± 19.97	94.91 ± 42.91	127.10 ± 25.6	170.90 ± 46.54	86.42 ± 20.21	46.92 ± 16.20
Trunk	76.67 ± 23.68	47.48 ± 18.35	51.59 ± 22.63	44.78 ± 6.82	106.23 ± 32.52	66.68 ± 18.79
Root	118.49 ± 13.24	105.80 ± 40.82	67.65 ± 18.79	23.58 ± 10.57	170.40 ± 36.49	44.55 ± 15.15

522

523   **3.3 Woody biomass and total NSCs on a global scale**

524

525   The average of the total GPP simulated from the new model during 1976–2005 was 123 PgC

526   year^{-1}. The model estimated the mean total woody biomass to be 282 PgC year^{-1} in boreal zones,

527   100 PgC year^{-1} in temperate zones, and 337 PgC year^{-1} in tropical zones globally during 1976–

528   2005. In boreal zones, the new model estimated the mean concentration of total NSCs to be 4.98%

529   ± 1.87% of total woody biomass, while the original SEIB-DGVM estimated it to be 6.37% ±

530   4.46% of total woody biomass (Fig. 5). The new model's estimation of the percentage of NSCs to

531   total woody biomass in North America and North Russia was lower than the original SEIB-

532   DGVM. In temperate zones, the mean concentration of total NSCs was 4.67% ± 0.54% of total

533   woody biomass from the new model, while 2.09% ± 1.59% from the original SEIB-DGVM. The

534   NSCs in the temperate forests of Asia and South America accounted for a larger fraction of total

535   biomass in the new model compared to the original SEIB-DGVM. Total NSCs of tropical forests

536   in South America and Africa from the new model were 6.19% ± 1.66% of their total woody

537   biomass, the original SEIB-DGVM estimated it to be 1.66% ± 1.02% of the total biomass. The

538   new model estimated a larger percentage of NSC to total biomass across tropical regions compared to

539   the original SEIB-DGVM.

540   Mean values of the simulated total NSCs relative to total woody biomass from the new model
541   were close to previous estimates for temperate and tropical forests (Table 6). The total NSCs of
542   temperate, broad-leaved, evergreen forests from the new model were 4.63% ± 0.50%, which
543   corresponded to the woody biomass reported by Smith et al. (2018). Furthermore, in the new model,
544   the total NSCs of temperate conifer forests were 4.72% ± 0.58% of total woody biomass, which was
545   close to the figure of 4% reported by Körner (2003). While, the original SEIB-DGVM calculated the
546   total NSCs of temperate broad-leaved evergreen forests to be 2.64% ± 1.24%, and the total NSCs of
547   temperate conifer forests were 5.30% ± 2.68% of the total woody biomass, which closely matched
548   the observations. However, the original SEIB-DGVM only considered NSCs in the trunks, whereas
549   the new model allocates the total NSC into three organs, resulting in a close match to the observed
550   total NSC. According to Würth et al. (2005), the percentages of woody biomass contributed by
551   NSCs are 4%–8% in tropical forests. The new model calculated to be 4.66% ± 1.28% in tropical
552   deciduous forests, and 7.11% ± 1.08% in tropical evergreen forests. In contrast, the total NSCs of
553   tropical deciduous forests from the original SEIB-DGVM were 1.66% ± 1.35% and the total
554   NSCs of tropical evergreen forests were 1.66% ± 0.71%, which were different from the observed
555   values. These observed percentages are close to our simulated values from the new model.
556
557   **Table 6.** Comparison of modeled mean NSC concentrations to observed total NSC concentrations (%)
558   for different types of biomes. The simulated results are expressed as the mean ± 1 standard deviation

	Total NSC	Leaf	Trunk	Root	Total NSC (Original SEIB-DGVM)	Observation
Boreal deciduous	3.41 ± 1.58	0.05 ± 0.09	3.06 ± 1.23	0.30 ± 0.62	2.47 ± 3.32	
Boreal evergreen	6.06 ± 1.16	0.75 ± 0.38	4.73 ± 1.29	0.58 ± 0.37	7.24 ± 4.22	
Temperate deciduous	2.30 ± 0.33	0.02 ± 0.01	2.25 ± 0.31	0.03 ± 0.01	1.45 ± 0.93	1.0–12.5 (Gough et al., 2009)
Temperate broad-leaved evergreen	4.63 ± 0.50	0.49 ± 0.20	4.10 ± 0.56	0.04 ± 0.03	2.64 ± 1.24	2.6–4.4 (Smith et al., 2018)
Temperate conifer	4.72 ± 0.58	0.89 ± 0.38	3.77 ± 0.73	0.08 ± 0.04	5.30 ± 2.68	4.0 (Körner, 2003)

Tropical deciduous	4.66 ± 1.28	0.04 ± 0.03	4.60 ± 1.27	0.03 ± 0.02	1.66 ± 1.35	4.0‑8.0 (Würth et al., 2005)
Tropical evergreen	7.11 ± 1.08	0.08 ± 0.03	7.00 ± 1.08	0.02 ± 0.01	1.66 ± 0.71	4.0–8.0 (Würth et al., 2005)

559

560
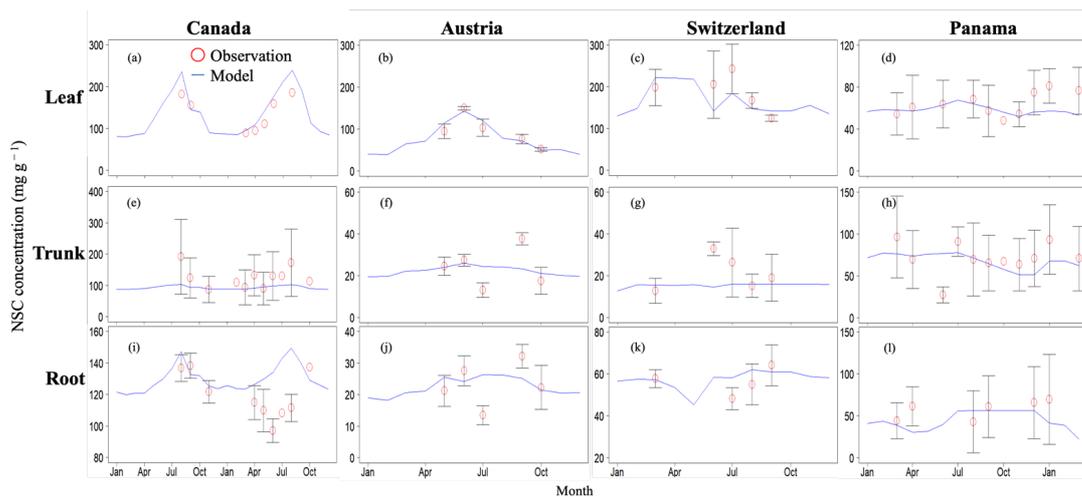
Figure 2. Validation of the modeled NSC with observed NSC data (mg g^{-1}) at sites in Canada,
Austria, Switzerland, and Panama. Red circles indicate the observed data, and blue lines indicate
the modeled NSC. The observed results are represented as mean ± 1 standard deviation. Observed
data are derived from Martínez-Vilalta et al. (2016)

565

566
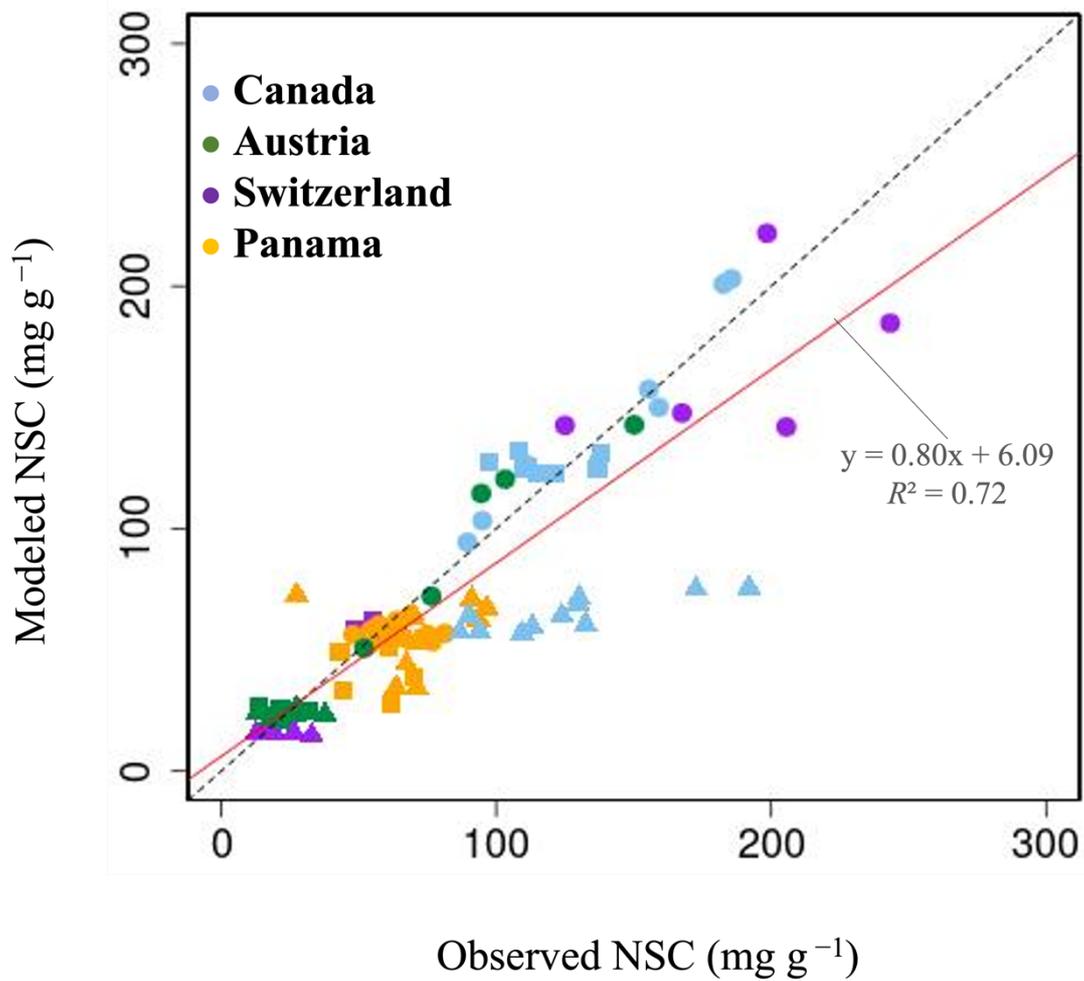
Figure 3. Plot of modeled NSC (mg g^{-1}) with observed NSC (mg g^{-1}) at a point scale. ●, leaves;
▲, trunks; ■, roots. For all data, *r* is 0.72, and RMSE is 29.65 mg g^{-1}.

569

570
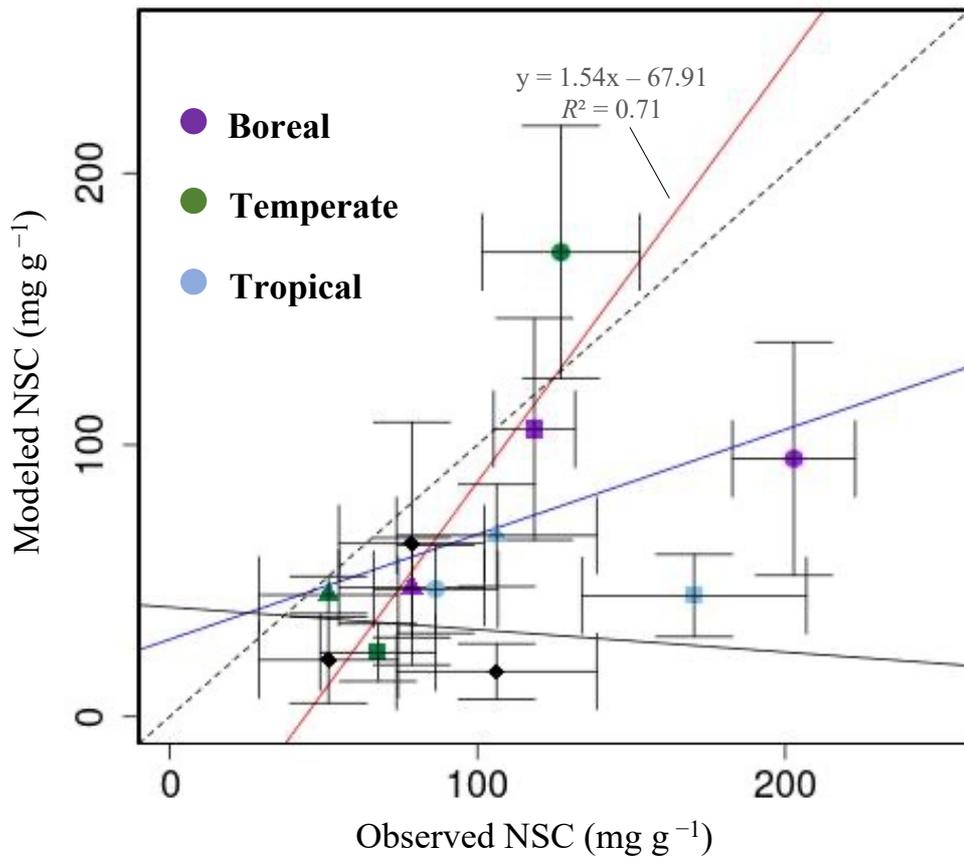
Figure 4. Plot of modeled NSC (mg g^{-1}) with observed NSC (mg g^{-1}) at a global scale. ●, leaves;
▲, trunks; ■, roots; ◆, trunks in the original SEIB-DGVM. Red line represents the regression
line of the plot that compares the modeled NSC from the new model with the observed NSC,
except for the NSCs of tree leaves in boreal forests and of tree roots in tropical forests. Blue line
represents the regression line of all plot from the new model with the observed NSC. Black solid
line represents the regression line of modeled NSC from the original SEIB-DGVM with the
observed NSC.

578
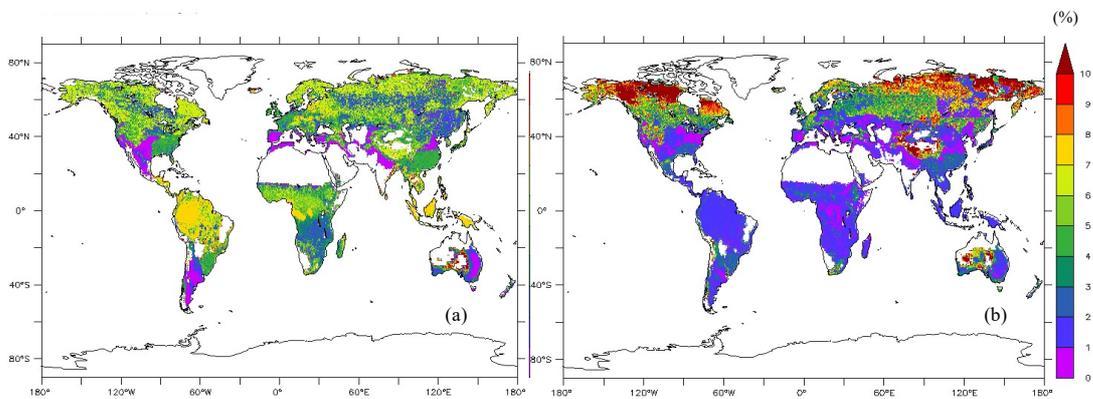
579

580   **Figure 5.** The global map of percentage of total NSC concentration relative to total dry woody

581   biomass averaged during 1976–2005 (%) (a) from the new model (b) from the original SEIB-

582   DGVM.

583

584

4 Discussion

At the point scale, the modeled NSCs for boreal forests in Canada were close to the observed NSCs. The seasonality of the modeled NSCs in leaves was consistent with observations. However, the seasonality of NSC in roots differed from the observations because there were insufficient observations in boreal regions that enabled assessment of the seasonality of NSCs in all organs. The seasonality of NSCs in roots is therefore still unclear. In temperate zones, the model simulated the observed NSCs very accurately. The simulated NSCs of temperate forests were close to observed values in Austria and Switzerland. The simulations showed that the NSCs in leaves were consumed in winter for bud flush, and the leaves accumulated NSCs during the growing season. This pattern corresponded to the seasonality reported in Asaadi et al. (2018) and Furze et al. (2019). In the tropical zones, the model also captured a seasonality of NSCs that was similar to observations. The NSC concentration in the canopy of tropical forests decreased from June to August to satisfy increased maintenance demands (Signori-Müller et al., 2022; Würth et al., 2005). The simulated NSCs in leaves followed a similar pattern from June to August, and the simulated NSCs in leaves, trunks, and roots were close to observed values.

At the global scale, the new model simulated NSC values in each organ of all climate regions that agreed with the observed data, except for the leaves of boreal forests and roots of tropical forests. As for the total NSCs of biome types, the modeled total NSCs of all temperate and tropical biomes matched the observed ranges well. In contrast, the original SEIB-DGVM only calculated NSC in trunks, and the modeled NSC in trunks of temperate and tropical forests were underestimated compared to observations. Total NSCs of tropical biomes were lower than observations, while those of temperate biomes were close to observations, but the original SEIB-DGVM did not assign the total NSC into leaves and roots. Therefore, these findings reveal that the new model can simulate NSC more accurately than the original SEIB-DGVM. In the original SEIB-DGVM, the NSC in trunks depended on the existing leaf biomass, which could not be applied to all biome types and climate zones, especially tropical forests. In the new model, the NSC_{organ} is determined by the biomass of the organ and photosynthesis in some climate zones. The new function, which was validated at the point scale, could therefore perform well on a global scale. The NSCs in trunks, which contain the greatest amounts of carbon in trees, were simulated accurately in all climate regions. The new function could therefore calculate the total NSCs in trees with great accuracy.

The model with the new function calculated the global GPP to be 123 PgC year^{-1}, which is close to the previous estimates of 106.2 ± 2.9 PgC year^{-1} by Zheng et al. (2020) and 130 ± 1.6 PgC year^{-1} by Madani et al. (2020). Moreover, the simulated mean total woody biomass for boreal forests was 282 PgC year^{-1}, which is within the range of 249–295 PgC year^{-1} reported by Pan et

621   al. (2011). The simulated woody biomass of 100 PgC year^{-1} for temperate forests was within the

622   observed range of 59–139 PgC year^{-1} (Hui et al., 2020) and a little lower than the range of 113–

623   125 PgC year^{-1} for other temperate forests (Pan et al., 2011). The calculated total woody biomass

624   of 337 PgC year^{-1} for tropical forests was within the range of 212–340 PgC year^{-1} reported by

625   Hui et al. (2020) and was not very different from the estimates of 378–564 PgC year^{-1} by Pan et

626   al. (2011), and 200–300 PgC year^{-1} by Mitchard (2018). Furthermore, the total NSCs relative to

627   total biomass output from the new function for temperate and tropical biome types agreed with

628   previous research. The total NSC of boreal biome types could not be compared with observations

629   due to lack of data.

630   The new model allows for simulation of various biotic effects on terrestrial ecosystems by

631   calculating the NSC dynamics within each plant organ. The NSCs stored in the trunk and roots

632   help to compensate for the deficit of CO_2 uptake in trees under stress, and the NSC stored in roots

633   is potentially indispensable for tree recovery after disturbances (Herrera-Ramírez et al., 2020).

634   Therefore, the NSC changes in the trunk and roots provide better indicators of carbon source–

635   sink relationships under elevated CO_2 conditions and are more closely related to the carbon

636   balance of plant bodies (Körner, 2003). While the original SEIB-DGVM was unable to simulate

637   biotic effects due to the lack of consideration for NSCs in all organs, simulation of the dynamics

638   of NSC in the three compartments in this research contributes to a better understanding plant

639   growth and the response of carbon dynamics in each organ to increasing atmospheric CO_2.

640   Carbon starvation may also be one of the causes of plant death during drought when

641   photosynthesis decreases and water stress increases (McDowell et al., 2008). If reduced

642   photosynthetic rates cannot supply enough carbon for NSC accumulation during drought, there

643   will be greater canopy dieback in the next season (McDowell, 2011; Chen et al., 2017). The new

644   model can simulate the dieback of long-lived temperate and tropical forests during drought,

645   because it can represent the total NSC in plant bodies at a global scale. Additionally, insect pests

646   have a significant impact on forest ecosystems, especially in temperate biomes, and their

647   outbreaks have increased with climate change (Canelles et al., 2021). To recover from defoliation

648   caused by insect pests and avoid decreased growth rates and lower survival rates, plants allocate

649   carbon for NSC defense mechanisms. The new model accurately simulates the amount of total

650   NSCs in temperate biomes, and therefore, it can be used to estimate the impact of insect pests on

651   a global and future scale.

652   The new model introduced NSC compartments in leaves, trunk, and roots that were validated

653   at the point and global scales. Use of the model developed here enabled simulation of the

654   environmental effects on forests resulting from the changing amount of NSC in each organ. The

655   simulations depicted the amount of NSC in the trunk at a global scale especially well, which

656   constitutes a significant portion of the total NSC. The model could thus be used as an indicator of

657   the carbon cycle in terrestrial ecosystems to understand the effect of climate change. Simulation
658   of photosynthetic carbon allocated into NSC storage in leaves, trunks, and roots enables a more
659   dynamic simulation of the carbon cycle between terrestrial ecosystems and the atmosphere.

660   However, there were still some limitations to this research. We considered two potential
661   limitations that could lead to some discrepancies between the modeled and measured NSC values.
662   First, the relatively coarse spatial resolution of 0.5°×0.5° gridded climate data at the global scale
663   could not depict the details of local climates derived from observations. These differences were
664   especially important in the case of temperature and short radiation, which play a key role in NSC
665   dynamics. Temperature surrounding plants is a key factor for the rate of plant growth (Hatfield
666   and Prueger, 2015). And different plant species has a specific temperature range. The short
667   radiation is used for a calculation of photosynthesis rate. These differences of two parameters
668   between 0.5°×0.5° gridded climate data and local climate data affect the ability of the trees to
669   accumulate NSCs.

670   Second, the scarcity of ground-measured NSC seasonality prevented us from having more
671   average information on NSC concentrations, especially in the tropical and boreal regions, where
672   there were fewer available data. The NSC seasonality differs between biome types, but because
673   it is difficult to measure NSC dynamics, there is a lack of long-term data for each biome type.
674   Hence, we adjusted the new NSC process and its related parameters based on climate zones rather
675   than biome types in our study. The fact that the NSC allocation was further influenced by
676   environmental conditions caused the allocation patterns to change within the same biome type.
677   The NSC allocation to roots was favored over aboveground allocations when soil resources were
678   lacking, and tree size was considered an important determinant of carbon allocation as well as
679   aridity (Hartmann et al., 2020). As we used data from different measurement sites for global-scale
680   validation, we could not account for the potential influence of varying surrounding conditions on
681   the data collected. In addition to the above factors, the number of samples and duration of
682   observations differed between the various studies. These differences led to no explicit NSC
683   seasonality. These potential sources of error in the field measurements jeopardized the model
684   performances.

685
686   **5 Conclusions**
687
688   In this study, a new NSC model was incorporated into the SEIB-DGVM to understand the effect
689   of NSC allocation on global forest dynamics through competition and establishment among
690   individual trees. The new module calculated the NSC dynamics of three organs—leaves, trunk,
691   and roots—and the general NSC seasonality based on ground measurements was determined for
692   biome types in three climate zones: boreal, temperate, and tropical. The NSC seasonality was

693 validated at four sites: Canada (boreal), Austria and Switzerland (temperate), and Panama

694 (tropical). The mean values of simulated NSC concentration agreed reasonably well with

695 observed data on a global scale.

696   The model enabled us to simulate the biotic effects resulting from insufficient NSC caused

697 by factors such as carbon starvation and insect pests that are otherwise difficult to measure in

698 terrestrial ecosystems globally. The difference of the NSC dynamics in the organs under

699 elevated CO_2 conditions highlighted the importance of modeling the organs separately when

700 studying environmental stresses. As more observation data about NSC dynamics become

701 available, the model can be further improved and can contribute to the simulations of the

702 passive biome shifts that may occur globally.

703

704 *Code and data availability*

705 The model code used in this study is archived at https://doi.org/10.5281/zenodo.7021459.

706

707 *Author contributions*. T.K. conceived and supervised this study and acquired the funding. H.N.

708 developed the model code and carried out the analysis and produced the figures. H.N. prepared

709 the original draft, and T.K., and L.V. reviewed it. L.W. prepared the modeling environment. All

710 authors have read and agreed to the published version of the manuscript.

711

712 *Competing interests*. The authors declare that they have no conflicts of interest.

713

714 *Acknowledgments*. This study was funded by the Nippon Life Insurance Company. This work

715 was supported by JSPS KAKENHI Grant Number JP 22J20286.

716 We thank all the contributors. Dr. Epron and Dr. Dannoura in Kyoto University provided

717 assistance. Dr. Hajima and Dr. Mori converted MIROC and CRU/NCEP climate data for

718 CRU/NCEP/MIROC integrated data. We acknowledge the data provided by the European Climate

719 Assessment & Dataset project.

720

References

721

722

723 Adams, H. D., Germino, M. J., Breshears, D. D., Barron-Gafford, G. A., Guardiola-Claramonte,

724   M., Zou, C. B. and Huxman, T. E.: Nonstructural leaf carbohydrate dynamics of *Pinus edulis*

725   during drought-induced tree mortality reveal role for carbon metabolism in mortality

726   mechanism, New Phytol., 197(4), 1142–1151, doi:10.1111/nph.12102, 2013.

727

728 Adams, H. D., Zeppel, M. J. B., Anderegg, W. R. L., Hartmann, H., Landhäusser, S. M., Tissue,

D. T., Huxman, T. E., Hudson, P. J., Franz, T. E., Allen, C. D., Anderegg, L. D. L., Barron-Gafford, G. A., Beerling, D. J., Breshears, D. D., Brodribb, T. J., Bugmann, H., Cobb, R. C., Collins, A. D., Dickman, L. T., Duan, H., Ewers, B. E., Galiano, L., Galvez, D. A., Garcia-Forner, N., Gaylord, M. L., Germino, M. J., Gessler, A., Hacke, U. G., Hakamada, R., Hector, A., Jenkins, M. W., Kane, J. M., Kolb, T. E., Law, D. J., Lewis, J. D., Limousin, J. M., Love, D. M., Macalady, A. K., Martínez-Vilalta, J., Mencuccini, M., Mitchell, P. J., Muss, J. D., O'Brien, M. J., O'Grady, A. P., Pangle, R. E., Pinkard, E. A., Piper, F. I., Plaut, J. A., Pockman, W. T., Quirk, J., Reinhardt, K., Ripullone, F., Ryan, M. G., Sala, A., Sevanto, S., Sperry, J. S., Vargas, R., Vennetier, M., Way, D. A., Xu, C., Yepez, E. A. and McDowell, N. G.: A multi-species synthesis of physiological mechanisms in drought-induced tree mortality, Nat. Ecol. Evol., 1(9), 1285–1291, doi:10.1038/s41559-017-0248-x, 2017.

Asaadi, A., Arora, V. K., Melton, J. R. and Bartlett, P.: An improved parameterization of leaf area index (LAI) seasonality in the Canadian Land Surface Scheme (CLASS) and Canadian Terrestrial Ecosystem Model (CTEM) modelling framework, Biogeosciences, 15(22), 6885–6907, doi:10.5194/bg-15-6885-2018, 2018.

Braakhekke, M. C., Doelman, J. C., Baas, P., Müller, C., Schaphoff, S., Stehfest, E. and Van Vuuren, D. P.: Modeling forest plantations for carbon uptake with the LPJmL dynamic global vegetation model, Earth Syst. Dyn., 10(4), 617–630, doi:10.5194/esd-10-617-2019, 2019.

Brutsaert, W.: On a derivable formula for long‑wave radiation from clear skies, Water Resour. Res., 11(5), 742‑744, doi:10.1029/WR011i005p00742, 1975.

Carbone, M. S., Czimczik, C. I., Keenan, T. F., Murakami, P. F., Pederson, N., Schaberg, P. G., Xu, X. and Richardson, A. D.: Age, allocation and availability of nonstructural carbon in mature red maple trees, New Phytol., 200(4), 1145–1155, doi:10.1111/nph.12448, 2013.

Canelles, Q., Aquilué, N., James, P. M. A., Lawler, J., and Brotons, L.: Global review on interactions between insect pests and other forest disturbances, Landsc. Ecol., 36(4), 945–972, https://doi.org/10.1007/s10980-021-01209-7, 2021.

Chen, Z., Wang, L., Dai, Y., Wan, X. and Liu, S.: Phenology-dependent variation in the non-structural carbohydrates of broadleaf evergreen species plays an important role in determining tolerance to defoliation (or herbivory), Sci. Rep., 7(1), 1–11, doi:10.1038/s41598-017-09757-2, 2017.

765

Chuste, P. A., Maillard, P., Bréda, N., Levillain, J., Thirion, E., Wortemann, R. and Massonnet, C.: Sacrificing growth and maintaining a dynamic carbohydrate storage are key processes for promoting beech survival under prolonged drought conditions, Trees - Struct. Funct., 34(2), 381–394, doi:10.1007/s00468-019-01923-5, 2020.

Dietze, M. C., Sala, A., Carbone, M. S., Czimczik, C. I., Mantooth, J. A., Richardson, A. D. and Vargas, R.: Nonstructural carbon in woody plants, Annu. Rev. Plant Biol., 65(June 2014), 667–687, doi:10.1146/annurev-arplant-050213-040054, 2014.

Furze, M. E., Huggett, B. A., Aubrecht, D. M., Stolz, C. D., Carbone, M. S. and Richardson, A. D.: Whole-tree nonstructural carbohydrate storage and seasonal dynamics in five temperate species, New Phytol., 221(3), 1466–1477, doi:10.1111/nph.15462, 2019.

Gough, C. M., Flower, C. E., Vogel, C. S. and Curtis, P. S.: Phenological and temperature controls on the temporal non-structural carbohydrate dynamics of *Populus grandidentata* and *Quercus rubra*, Forests, 1(1), 65–81, doi:10.3390/f1010065, 2010.

Gough, C. M., Flower, C. E., Vogel, C. S., Dragoni, D. and Curtis, P. S.: Whole-ecosystem labile carbon production in a north temperate deciduous forest, Agric. For. Meteorol., 149(9), 1531–1540, doi:10.1016/j.agrformet.2009.04.006, 2009.

Gruber, A., Pirkebner, D., Oberhuber, W. and Wieser, G.: Spatial and seasonal variations in mobile carbohydrates in Pinus cembra in the timberline ecotone of the Central Austrian Alps, Eur. J. For. Res., 130(2), 173–179, doi:10.1007/s10342-010-0419-7, 2011.

Gruber, A., Pirkebner, D., Florian, C. and Oberhuber, W.: No evidence for depletion of carbohydrate pools in Scots pine (Pinus sylvestris L.) under drought stress, Plant Biol., 14(1), 142–148, doi:10.1111/j.1438-8677.2011.00467.x, 2012.

Harris, I., P. D. Jones, T. J. Osborn, and D. H. Lister: Updated high-resolution grids of monthly climatic observations - the CRU TS3.10 Dataset, Int. J. Climatol., 34(3), 623-642, doi:10.1002/joc.3711, 2014.

Hartmann, H., Adams, H. D., Hammond, W. M., Hoch, G., Landhäusser, S. M., Wiley, E. and Zaehle, S.: Identifying differences in carbohydrate dynamics of seedlings and mature trees to

801   improve carbon allocation in models for trees and forests, Environ. Exp. Bot., 152(September
802   2017), 7–18, doi:10.1016/j.envexpbot.2018.03.011, 2018.
803
804   Hartmann, H., Bahn, M., Carbone, M. and Richardson, A. D.: Plant carbon allocation in a
805   changing world – challenges and progress: introduction to a Virtual Issue on carbon
806   allocation: Introduction to a virtual issue on carbon allocation, New Phytol., 227(4), 981–988,
807   doi:10.1111/nph.16757, 2020.
808
809   Hatfield, J. L. and Prueger, J. H.: Temperature extremes: Effect on plant growth and development,
810   Weather Clim. Extrem., 10, 4–10, https://doi.org/10.1016/j.wace.2015.08.001, 2015.
811
812   He, W., Liu, H., Qi, Y., Liu, F. and Zhu, X.: Patterns in nonstructural carbohydrate contents at the
813   tree organ level in response to drought duration, Glob. Chang. Biol., 26(6), 3627–3638,
814   doi:10.1111/gcb.15078, 2020.
815
816   Herrera-Ramírez, D., Muhr, J., Hartmann, H., Römermann, C., Trumbore, S. and Sierra, C. A.:
817   Probability distributions of nonstructural carbon ages and transit times provide insights into
818   carbon allocation dynamics of mature trees, New Phytol., 226(5), 1299 ‐ 1311,
819   doi:10.1111/nph.16461, 2020.
820
821   Hickler, T., Smith, B., Sykes, M. T., Davis, M. B., Sugita, S. and Walker, K.: Using a generalized
822   vegetation model to simulate vegetation dynamics in northeastern USA, Ecology, 85(2), 519–
823   530, doi:10.1890/02-0344, 2004.
824
825   Hoch, G., Richter, A. and Körner, C.: Non-structural carbon compounds in temperate forest trees,
826   Plant, Cell Environ., 26(7), 1067–1081, doi:10.1046/j.0016-8025.2003.01032.x, 2003.
827
828   Huang, J., Kautz, M., Trowbridge, A. M., Hammerbacher, A., Raffa, K. F., Adams, H. D.,
829   Goodsman, D. W., Xu, C., Meddens, A. J. H., Kandasamy, D., Gershenzon, J., Seidl, R. and
830   Hartmann, H.: Tree defence and bark beetles in a drying world: carbon partitioning,
831   functioning and modelling, New Phytol., 225(1), 26–36, doi:10.1111/nph.16173, 2020.
832
833   Hui, D., Deng, Q., Tian, H. and Luo, Y.: Handbook of Climate Change Mitigation and Adaptation.,
834   2020.
835
836   IPCC: 2014: Climate Change 2014: Synthesis Report. Contribution of Working Groups I, II and

837   III to the Fifth Assessment Report of the Intergovernmental Panel on Climate Change, edited
838   by: Core Writing Team, Pachauri, R. K., and Meyer, L. A., IPCC, Geneva, Switzerland, 2014.

839

840   Jones, S., Rowland, L., Cox, P., Hemming, D., Wiltshire, A., Williams, K., Parazoo, N., Liu, J.,
841   da Costa, A., Meir, P., Mencuccini, M. and Harper, A.: The Impact of a Simple Representation
842   of Non-Structural Carbohydrates on the Simulated Response of Tropical Forests to Drought,
843   Biogeosciences Discuss., 1–26, doi:10.5194/bg-2019-452, 2019.

844

845   Kalnay, E., Kanamitsu, M., Kistler, R., Collins, W., Deaven, D., Gandin, L., Iredell, M.,
846   Saha, S., White, G., Woollen, J., Zhu, Y., Chelliah, M., Ebisuzaki, W., Higgins, W.,
847   Janowiak, J., Mo, K. C., Ropelewski, C., Wang, J., Leetmaa, A., Reynolds, R.,
848   Jenne, R., & Joseph, D.: The NCEP/NCAR 40-Year Reanalysis Project, Bulletin of
849   the American Meteorological Society, 77(3), 437-472. 1996

850

851   Klein, T. and Hoch, G.: Tree carbon allocation dynamics determined using a carbon mass balance
852   approach, New Phytol., 205(1), 147–159, doi:10.1111/nph.12993, 2015.

853

854   Klein Tank, A.M.G. and Coauthors, 2002. Daily dataset of 20th-century surface air temperature
855   and precipitation series for the European Climate Assessment. Int. J. of Climatol., 22, 1441-
856   1453.

857

858   Körner, C.: Carbon limitation in trees, J. Ecol., 91(1), 4–17, doi:10.1046/j.1365-
859   2745.2003.00742.x, 2003.

860

861   Krinner, G., Viovy, N., de Noblet-Ducoudré, N., Ogée, J., Polcher, J., Friedlingstein, P., Ciais, P.,
862   Sitch, S. and Prentice, I. C.: A dynamic global vegetation model for studies of the coupled
863   atmosphere-biosphere system, Global Biogeochem. Cycles, 19(1), 1–33,
864   doi:10.1029/2003GB002199, 2005.

865

866   Landhäusser, S. M. and Lieffers, V. J.: Seasonal changes in carbohydrate reserves in mature
867   northern Populus tremuloides clones, Trees - Struct. Funct., 17(6), 471–476,
868   doi:10.1007/s00468-003-0263-1, 2003.

869

870   Madani, N., Parazoo, N. C., Kimball, J. S., Ballantyne, A. P., Reichle, R. H., Maneta, M., Saatchi,
871   S., Palmer, P. I., Liu, Z. and Tagesson, T.: Recent Amplified Global Gross Primary
872   Productivity Due to Temperature Increase Is Offset by Reduced Productivity Due to Water

873   Constraints, AGU Adv., 1(4), doi:10.1029/2020av000180, 2020.

874

875   Martínez-Vilalta, J., Sala, A., Asensio, D., Galiano, L., Hoch, G., Palacio, S., Piper, F. I. and Lloret,

876   F.: Dynamics of non-structural carbohydrates in terrestrial plants: A global synthesis, Ecol.

877   Monogr., 86(4), 495–516, doi:10.1002/ecm.1231, 2016.

878

879   McDowell, N., Pockman, W. T., Allen, C. D., Breshears, D. D., Cobb, N., Kolb, T., Plaut, J.,

880   Sperry, J., West, A., Williams, D. G. and Yepez, E. A.: Mechanisms of plant survival and

881   mortality during drought: Why do some plants survive while others succumb to drought?,

882   New Phytol., 178(4), 719–739, doi:10.1111/j.1469-8137.2008.02436.x, 2008.

883

884   McDowell, N. G.: Mechanisms linking drought, hydraulics, carbon metabolism, and vegetation

885   mortality, Plant Physiol., 155(3), 1051–1059, doi:10.1104/pp.110.170704, 2011.

886

887   McDowell, N. G., Allen, C. D., Anderson-Teixeira, K., Aukema, B. H., Bond-Lamberty, B., Chini,

888   L., Clark, J. S., Dietze, M., Grossiord, C., Hanbury-Brown, A., Hurtt, G. C., Jackson, R. B.,

889   Johnson, D. J., Kueppers, L., Lichstein, J. W., Ogle, K., Poulter, B., Pugh, T. A. M., Seidl, R.,

890   Turner, M. G., Uriarte, M., Walker, A. P. and Xu, C.: Pervasive shifts in forest dynamics in a

891   changing world, Science (80-.)., 368(6494), doi:10.1126/science.aaz9463, 2020.

892

893   Mitchard, E. T. A.: The tropical forest carbon cycle and climate change, Nature, 559(7715), 527–

894   534, doi:10.1038/s41586-018-0300-2, 2018.

895

896   Pan, Y., Birdsey, R. A., Fang, J., Houghton, R., Kauppi, P. E., Kurz, W. A., Phillips, O. L.,

897   Shvidenko, A., Lewis, S. L., Canadell, J. G., Ciais, P., Jackson, R. B., Pacala, S. W.,

898   McGuire, A. D., Piao, S., Rautiainen, A., Sitch, S., and Hayes, D.: A large and persistent

899   carbon sink in the world's forests, Science (1979), 333, 988–993,

900   doi:10.1126/science.1201609, 2011.

901

902   Rademacher, T., Fonti, P., LeMoine, J. M., Fonti, M. V., Basler, D., Chen, Y., Friend, A. D.,

903   Seyednasrollah, B., Eckes-Shephard, A. H. and Richardson, A. D.: Manipulating phloem

904   transport affects wood formation but not local nonstructural carbon reserves in an evergreen

905   conifer, Plant Cell Environ., 44(8), 2506–2521, doi:10.1111/pce.14117, 2021.

906

907   Richardson, A. D., Carbone, M. S., Keenan, T. F., Czimczik, C. I., Hollinger, D. Y., Murakami, P.,

908   Schaberg, P. G. and Xu, X.: Seasonal dynamics and age of stemwood nonstructural

909   carbohydrates in temperate forest trees, New Phytol., 197(3), 850–861,
910   doi:10.1111/nph.12042, 2013.

911

912   Sala, A., Woodruff, D. R. and Meinzer, F. C.: Carbon dynamics in trees: Feast or famine?, Tree
913   Physiol., 32(6), 764–775, doi:10.1093/treephys/tpr143, 2012.

914

915   Sato, H. and Ise, T.: Effect of plant dynamic processes on African vegetation responses to climate
916   change: Analysis using the spatially explicit individual-based dynamic global vegetation
917   model (SEIB-DGVM), J. Geophys. Res. Biogeosciences, 117(3), 1–18,
918   doi:10.1029/2012JG002056, 2012.

919

920   Sato, H., Itoh, A. and Kohyama, T.: SEIB-DGVM: A new Dynamic Global Vegetation Model
921   using a spatially explicit individual-based approach, Ecol. Modell., 200(3–4), 279–307,
922   doi:10.1016/j.ecolmodel.2006.09.006, 2007.

923

924   Sato, H., Kobayashi, H., Beer, C. and Fedorov, A.: Simulating interactions between topography,
925   permafrost, and vegetation in Siberian larch forest, Environ. Res. Lett., 15(9),
926   doi:10.1088/1748-9326/ab9be4, 2020.

927

928   Sato, H., Kobayashi, H., Iwahana, G., and Ohta, T.: Endurance of larch forest ecosystems in
929   eastern Siberia under warming trends, Ecol. Evol., 6, 5690–5704,
930   https://doi.org/10.1002/ece3.2285, 2016.

931

932   Seidl, R., Thom, D., Kautz, M., Martin-Benito, D., Peltoniemi, M., Vacchiano, G., Wild, J., Ascoli,
933   D., Petr, M., Honkaniemi, J., Lexer, M. J., Trotsiuk, V., Mairota, P., Svoboda, M., Fabrika, M.,
934   Nagel, T. A. and Reyer, C. P. O.: Forest disturbances under climate change, Nat. Clim. Chang.,
935   7(6), 395–402, doi:10.1038/nclimate3303, 2017.

936

937   Sevanto, S. and Dickman, L. T.: Where does the carbon go?-Plant carbon allocation under climate
938   change, Tree Physiol., 35(6), 581–584, doi:10.1093/treephys/tpv059, 2015.

939

940   Signori-Müller, C., Oliveira, R. S., Valentim Tavares, J., Carvalho Diniz, F., Gilpin, M., de V.
941   Barros, F., Marca Zevallos, M. J., Salas Yupayccana, C. A., Nina, A., Brum, M., Baker, T. R.,
942   Cosio, E. G., Malhi, Y., Monteagudo Mendoza, A., Phillips, O. L., Rowland, L., Salinas, N.,
943   Vasquez, R., Mencuccini, M. and Galbraith, D.: Variation of non-structural carbohydrates
944   across the fast–slow continuum in Amazon Forest canopy trees, Funct. Ecol., 36(2), 341–355,

945   doi:10.1111/1365-2435.13971, 2022.

946

947   Singh, K. P. and Srivastava, K.: Seasonal variation in the biomass and non-structural carbohydrate

948   content of fine roots of teak (Tectona grandis L. f.) plantations in a dry tropical region, Tree

949   Physiol., 1(1), 31–36, doi:10.1093/treephys/1.1.31, 1986.

950

951   Smith, B., Prentice, I. C. and Sykes, M. T.: Representation of vegetation dynamics in the

952   modelling of terrestrial ecosystems: Comparing two contrasting approaches within European

953   climate   space,   Glob.   Ecol.   Biogeogr.,   10(6),   621–637,   doi:10.1046/j.1466-

954   822X.2001.00256.x, 2001.

955

956   Smith, M. G., Miller, R. E., Arndt, S. K., Kasel, S., and Bennett, L. T.: Whole-tree distribution

957   and temporal variation of non-structural carbohydrates in broadleaf evergreen trees, Tree

958   Physiol, 38, 570–581, https://doi.org/10.1093/treephys/tpx141, 2018.

959

960   Stevens-Rumann, C. S., Kemp, K. B., Higuera, P. E., Harvey, B. J., Rother, M. T., Donato, D. C.,

961   Morgan, P. and Veblen, T. T.: Evidence for declining forest resilience to wildfires under

962   climate change, Ecol. Lett., 21(2), 243–252, doi:10.1111/ele.12889, 2018.

963

964   Sveinbjörnsson, B., Smith, M., Traustason, T., Ruess, R. W. and Sullivan, P. F.: Variation in

965   carbohydrate source-sink relations of forest and treeline white spruce in southern, interior and

966   northern Alaska, Oecologia, 163(4), 833–843, doi:10.1007/s00442-010-1597-1, 2010.

967

968   Tei, S., Sugimoto, A., Liang, M., Yonenobu, H., Matsuura, Y., Osawa, A., Sato, H., Fujinuma, J.

969   and Maximov, T.: Radial Growth and Physiological Response of Coniferous Trees to Arctic

970   Amplification,   J.   Geophys.   Res.   Biogeosciences,   122(11),   2786–2803,

971   doi:10.1002/2016JG003745, 2017.

972

973   Wang, Z., Zhou, Z. and Wang, C.: Defoliation-induced tree growth declines are jointly limited by

974   carbon   source   and   sink   activities,   Sci.   Total   Environ.,   762,   143077,

975   doi:10.1016/j.scitotenv.2020.143077, 2021.

976

977   Watanabe, S., Hajima, T., Sudo, K. and Nagashima, T.: MIROC-ESM: model description and

978   basic results of CMIP5-20c3m experiments, Geosci. Model Dev. Discuss., 4(2), 1063–1128,

979   doi:10.5194/gmdd-4-1063-2011, 2011.

980

981   Weedon, G. P., Balsamo, G., Bellouin, N., Gomes, S., Best, M. J., and Viterbo, P.: The WFDEI
982   Meteorological Forcing Data, Research Data Archive at the National Center for
983   Atmospheric Research, Computational and Information Systems Laboratory,
984   https://doi.org/10.5065/486N-8109, 2018. Accessed 11 Dec 2020.

985

986   Woodruff, D. R. and Meinzer, F. C.: Water stress, shoot growth and storage of non-structural
987   carbohydrates along a tree height gradient in a tall conifer, Plant, Cell Environ., 34(11), 1920–
988   1930, doi:10.1111/j.1365-3040.2011.02388.x, 2011.

989

990   Würth, M. K. R., Peláez-Riedl, S., Wright, S. J. and Körner, C.: Non-structural carbohydrate pools
991   in a tropical forest, Oecologia, 143(1), 11–24, doi:10.1007/s00442-004-1773-2, 2005.

992

993   Xu, C., Liu, H., Anenkhonov, O. A., Korolyuk, A. Y., Sandanov, D. V., Balsanova, L. D.,
994   Naidanov, B. B. and Wu, X.: Long-term forest resilience to climate change indicated by
995   mortality, regeneration, and growth in semiarid southern Siberia, Glob. Chang. Biol., 23(6),
996   2370–2382, doi:10.1111/gcb.13582, 2017.

997

998   Zheng, Y., Shen, R., Wang, Y., Li, X., Liu, S., Liang, S., Chen, J. M., Ju, W., Zhang, L. and Yuan,
999   W.: Improved estimate of global gross primary production for reproducing its long-Term
1000   variation, 1982-2017, Earth Syst. Sci. Data, 12(4), 2725–2746, doi:10.5194/essd-12-2725-
1001   2020, 2020.

1002